LETTERS
https://doi.org/10.1038/s41558-019-0561-2
nature climate change

Stabilization of dense Antarctic water supply to the Atlantic Ocean overturning circulation

E. Povl Abrahamsen[1*], Andrew J. S. Meijers[1], Kurt L. Polzin[2], Alberto C. Naveira Garabato[3], Brian A. King[4], Yvonne L. Firing[4], Jean-Baptiste Sallée[5], Katy L. Sheen[6], Arnold L. Gordon[7], Bruce A. Huber[7] and Michael P. Meredith[1]

The lower limb of the Atlantic overturning circulation is resupplied by the sinking of dense Antarctic Bottom Water (AABW) that forms via intense air–sea–ice interactions next to Antarctica, especially in the Weddell Sea[1]. In the last three decades, AABW has warmed, freshened and declined in volume across the Atlantic Ocean and elsewhere[2–7], suggesting an ongoing major reorganization of oceanic overturning[8,9]. However, the future contributions of AABW to the Atlantic overturning circulation are unclear. Here, using observations of AABW in the Scotia Sea, the most direct pathway from the Weddell Sea to the Atlantic Ocean, we show a recent cessation in the decline of the AABW supply to the Atlantic overturning circulation. The strongest decline was observed in the volume of the densest layers in the AABW throughflow from the early 1990s to 2014; since then, it has stabilized and partially recovered. We link these changes to variability in the densest classes of abyssal waters upstream. Our findings indicate that the previously observed decline in the supply of dense water to the Atlantic Ocean abyss may be stabilizing or reversing and thus call for a reassessment of Antarctic influences on overturning circulation, sea level, planetary-scale heat distribution and global climate[2,3,8].

Antarctic Bottom Water (AABW) occupies more than 35% of the volume of the global ocean[10] and the sinking of this dense water as it is formed around Antarctica plays a key role in driving the lower limb of the global overturning circulation[11]. The recently ventilated nature of AABW means that it can be influenced strongly by changes in surface forcing, with several landmark studies observing a poleward-intensified warming[3] and freshening[5–7] of AABW. These trends have been attributed to anthropogenically driven increases in glacial meltwater discharge and shifts in wind patterns reducing dense water formation rates and AABW export from Antarctic continental shelves[12]. However, due to the inaccessibility of these source regions, our ability to monitor such changes is mostly limited to repeat occupations of a few hydrographic sections situated mainly farther north.

Here, we use data from three of the most comprehensively sampled sections in the Southern Ocean, located in the Weddell and Scotia Seas: SR1b, which spans eastern Drake Passage south of the Falkland Islands; SR4, which crosses the Weddell Sea from Cape Norvegia on the coast of Queen Maud Land to Joinville Island off the tip of the Antarctic Peninsula; and A23, which extends from the northern Weddell Sea to South Georgia (Fig. 1). Since 1989 they have been partially or fully occupied 26, 9 and 12 times, respectively, placing them among the most useful sections for determining long-term changes in AABW properties and transports. The A23 section is particularly well-positioned to capture changes in the equatorward transport of AABW from its formation regions upstream in the Weddell Sea, since it spans the most direct export route via the Scotia Sea and is sufficiently far downstream from the AABW source regions that aliasing of seasonal water mass changes is minimized[13]. Following Meredith et al.[13] and Heywood et al.[14], we define the densest class of the AABW that is exported from the Weddell Sea as Lower Weddell Sea Deep Water (LWSDW), with a neutral density[15] (γ^n) between 28.31 and 28.40 kg m^{-3}. Orkney Passage, a 3,650-m-deep gap in the South Scotia Ridge (SSR), is the main export route of WSDW from the Weddell Sea to the Scotia Sea, accounting for almost all of the northward transport of LWSDW over the SSR and around one-quarter of all the transport of dense bottom waters from Antarctica to lower latitudes[16,17].

Figure 2 shows the area of LWSDW on the part of A23 that spans the Scotia Sea north of the SSR (at about 60° S) and on the SR1b section. Computation of these areas is described in more detail in Methods. The area occupied by LWSDW on A23 steadily and significantly declined by almost two-thirds from 1995 to 2014, in agreement with previous observations of dwindling AABW volumes in the South Atlantic[2] and further north[4,9]. Subsequently, from 2014 to 2018 LWSDW volume recovered to near its 2005 levels, remaining stable from 2016 to 2018.

The LWSDW area on SR1b (Fig. 2) also showed an overall downward trend from 1993 to 2014 and an increase in 2014 and 2015 but the area of LWSDW on this section is smaller, and its relative variability much larger, than on A23, thus hampering determination of whether the trend has reversed or flattened at SR1b. Except in 2014 and 2015, very little LWSDW has been observed on this section since 2009. The SR1b section is located to the west of the major routes of LWSDW export through the Scotia Sea and its interannual variability is related to other factors (including the movement of fronts in Drake Passage[18] and changes in the small amount of Weddell Sea export that occurs west of Orkney Passage[19]) that have weak or no influence on A23. We therefore conclude that the interannual variability at SR1b does not reflect changes in the water mass properties in the central Scotia Sea and that, although the SR1b record cannot unambiguously confirm the recovery and stabilization observed on A23, neither does it contradict it.

The decrease in volume of LWSDW in the Scotia Sea to 2014 and its pronounced recovery thereafter could be caused by: (1) changes in the rate of supply from its source regions upstream in

[1]British Antarctic Survey, Cambridge, UK. [2]Woods Hole Oceanographic Institution, Woods Hole, MA, USA. [3]University of Southampton, Southampton, UK. [4]National Oceanography Centre, Southampton, UK. [5]Sorbonne Université, CNRS, LOCEAN, Paris, France. [6]University of Exeter, Penryn, UK. [7]Lamont-Doherty Earth Observatory, Columbia University, Palisades, NY, USA. *e-mail: epab@bas.ac.uk

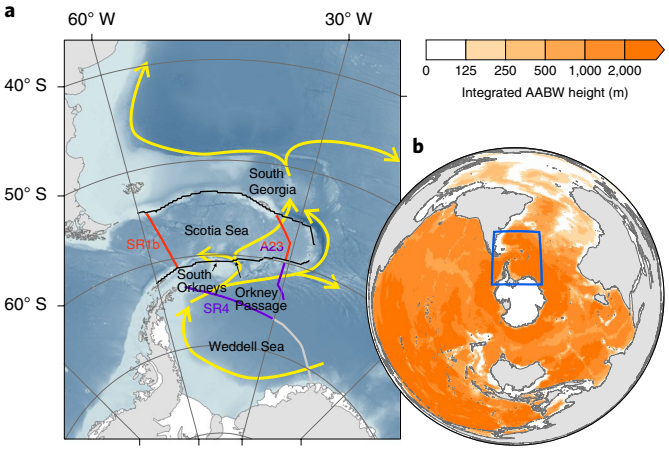

Fig. 1 | Pathways of AABW from the Weddell Sea into the world ocean. **a**, Map of the Scotia Sea, with the South and North Scotia Ridges marked by black lines. The SR1b section and the part of the A23 section in the Scotia Sea are marked in red. The parts of the A23 and SR4 sections in the Weddell Sea used here are marked in purple. Yellow arrows show schematic pathways of AABW from refs. [14,35,36]. The bathymetry data are from the GEBCO_2014 Grid, v. 20150318. **b**, Map showing the global extent (vertically integrated fraction) of AABW, based on the methods of Johnson[10] using updated data from the World Ocean Atlas 2013[37–40], on a Lambert azimuthal equal-area projection. The area shown in **a** is outlined in blue.

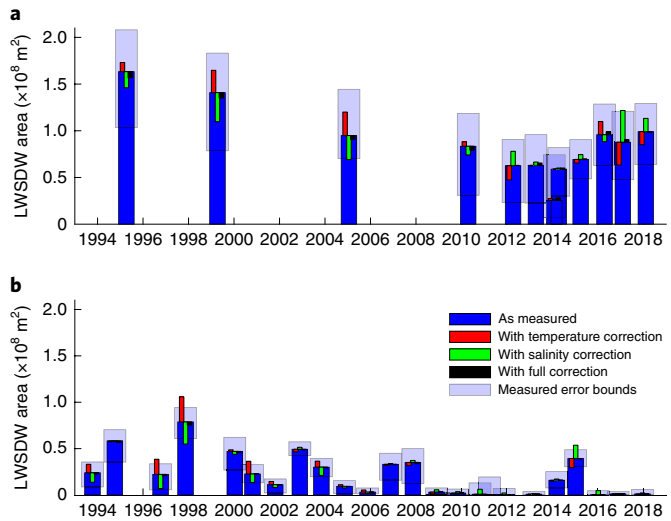

Fig. 2 | Area of LWSDW from hydrographic sections. a,**b**, Graphs showing LWSDW ($\gamma^n = 28.31\,kg\,m^{-3}$) areas from the A23 section in the Scotia Sea (**a**) and from the SR1b section (**b**). The blue bars are calculated from the measured properties; the red bars are compensated for the temperature anomalies on the $\gamma^n = 28.31\,kg\,m^{-3}$ surface (as shown in Supplementary Fig. 2 and discussed in more detail in Methods); the green bars are compensated for salinity anomalies; and the black bars are compensated for both temperature and salinity anomalies. Computation of the confidence limits (light blue bars) is described in the Methods.

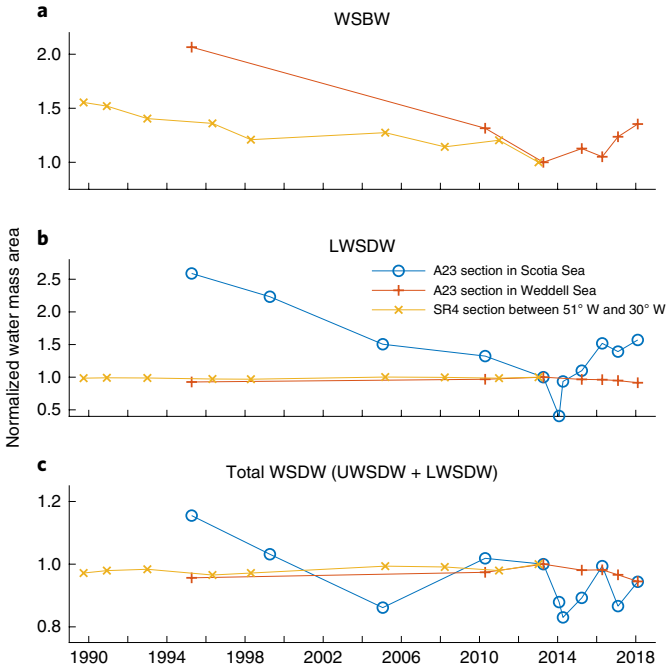

Fig. 3 | Normalized areas of water masses on hydrographic sections. **a**–**c**, Graphs showing data for WSBW, $\gamma^n > 28.40\,kg\,m^{-3}$ (**a**), LWSDW, $28.31 < \gamma^n < 28.40\,kg\,m^{-3}$ (**b**) and WSDW, $28.26 < \gamma^n < 28.40\,kg\,m^{-3}$ (**c**). Sections used are the A23 section in the Scotia Sea (blue circles; red section in Fig. 1) and the A23 and SR4 sections in the Weddell Sea (red and orange crosses; purple sections in Fig. 1). The values have been normalized such that the 2013 values are equal to 1.

the Weddell Sea; (2) changes in its properties, for example a reduction in density caused by warming or freshening with a consequent apparent decrease in the downstream observed fraction of the water mass; or (3) changes in the rate of its outflow from the Scotia Sea to lower-latitude regions. Our contention, discussed below and based on consideration of the changing water mass structure upstream in the Weddell Sea, is that possibility 1, just described, is the principal contributor and that this variability is driven by changes in the volume of denser water masses in the Weddell Sea.

We demonstrate upstream water mass structure change using hydrographic data from the western part of the SR4 section, west of 30° W and the part of the A23 section south of SSR and north of 64° S; these regions are marked in purple in Fig. 1. The western part of the SR4 section spans the flow of deep water from the Weddell Sea toward the passages where it can overflow the SSR and enter the Scotia Sea. The Weddell A23 segment is downstream of the flow into Orkney Passage but we postulate that it is representative of conditions in the northern and northwestern Weddell Sea as evidenced by the similarity in its variability with that of SR4. The upper boundary of LWSDW ($\gamma^n = 28.31\,kg\,m^{-3}$) in the Weddell Sea deepened progressively between the early 1990s and 2013 on both SR4 and the southern part of A23 (Supplementary Fig. 1); however, there has been no discernible change in the area of LWSDW on either section (Fig. 3), with the lowering of the LWSDW upper boundary entirely caused by a loss in area of the underlying Weddell Sea Bottom Water (WSBW; $\gamma^n > 28.40\,kg\,m^{-3}$), as observed on this section by Fahrbach et al.[20] and Purkey and Johnson[4]. The resulting deepening of the overlying LWSDW isopycnals in the Weddell Sea is consistent with a reduction in the export of LWSDW to the Scotia Sea and a reduction in the amount of LWSDW observed there, since a smaller depth range of the LWSDW density class will be able to clear the crest of Orkney Passage.

Similarly, the recent period of marked LWSDW recovery on A23 in the Scotia Sea coincided with recovery of WSBW on A23 in the Weddell Sea. While the SR4 record does not span this period, data from oceanographic moorings that have been deployed in Orkney Passage (Fig. 1) since 2004, with full coverage across the passage

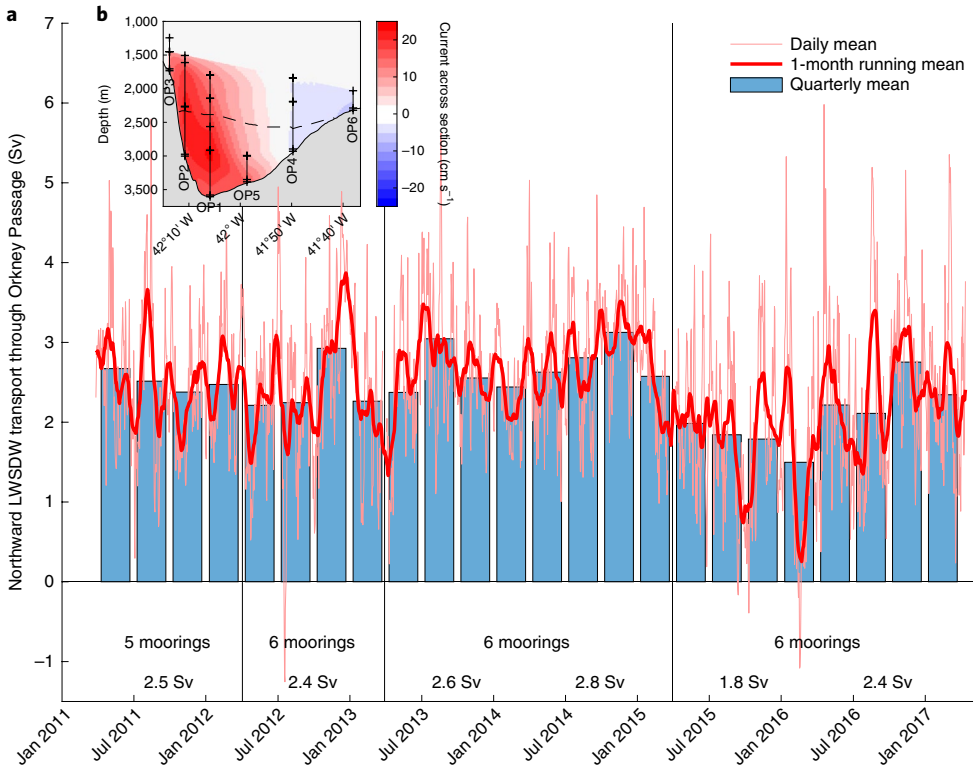

Fig. 4 | Northward transport of LWSDW through Orkney Passage. a, LWSDW ($\gamma^n > 28.31$ kg m^{-3}) volume transport: the light red line indicates daily averages of transport through the mooring array, the thick red line is the 1-month running mean and the blue bars are quarterly averages. Vertical black lines indicate mooring cruises to the area; the annual (1 April–31 March) mean LWSDW transport through the array is indicated at the bottom of the graph. **b**, The mean current across (normal to) the section is shown, with the location of the six moorings (labelled OP1–OP6) and the instruments deployed in 2013–2015 indicated. The dashed line shows the mean extent of LWSDW on the section.

since 2011, lend support to our proposition that the observed recovery of LWSDW is also due to changes in upstream flow. The northward LWSDW volume transport through Orkney Passage from 2011 to 2017 is shown in Fig. 4. This time series captures the period of the increasing LWSDW volume in the Scotia Sea. Transport of LWSDW in 2013–2015 was approximately 0.3 Sv (10^6 m^3 s^{-1}) larger than the long-term mean of 2.4 Sv; this difference is substantial even in the context of the large short-term variability that is present. The effect of a transport increase of 0.3 Sv over 2 yr would be an increase of between $8.1 \pm 1.7 \times 10^6$ m^2 and $2.3 \pm 0.5 \times 10^7$ m^2 in the area of LWSDW on the A23 section (see Methods). The upper bound of this estimate is comparable to the observed increase in A23 LWSDW area from 2014 to 2016, indicating that recovering Scotia Sea LWSDW volumes after 2014 may be plausibly attributed to increased LWSDW transport through Orkney Passage. The large decrease in transport in 2015–2016, a period during which the A23 LWSDW area remained stable, might appear contradictory; however, this probably reflects longer time scales for sinks (outflow or upward mixing) than for sources of LWSDW in the Scotia Sea, resulting in a lag before a decrease would be observed. Meredith et al.[13] estimate an approximately 3-yr residence time for LWSDW in the Scotia Sea.

We discuss the second and third mechanisms, and our rationales for discounting them as causes of the LWSDW changes on A23, more fully in Methods. In summary, we find that density effects of the observed freshening and cooling (possibility 2) cannot account for the changes in LWSDW area observed at A23 (red, green and black bars in Fig. 2 and Supplementary Fig. 2) and that the variation in eddy-driven mixing that would be needed to drive a marked increase in the rate of removal of LWSDW from the Scotia Sea[21,22] (possibility 3) is not supported by observations (Supplementary Fig. 3).

A natural question that follows from our inference of a reinvigorated LWSDW export from the Weddell Sea linked to WSBW recovery is: what has driven this change? Much recent work has focused on the role of winds over the Weddell Gyre as a cause of export variability, either increasing the baroclinicity of the gyre[13] or acting more locally on its northern boundary current to modify transports and isopycnal depths[23–26]. However, we do not see any clear signal in wind stress or its curl over either the Weddell Gyre or SSR that may explain the long-term LWSDW decline before 2014, nor a shift that might be associated with its recovery since then (Supplementary Fig. 4). Conceptual arguments presented by Meredith et al.[13] and Coles et al.[27] suggest that variations in the strength of the Weddell Gyre, forced by wind stress, may affect the inclination of isopycnals across the gyre, in turn controlling the range of water masses exported northward, and recent work has demonstrated that the cyclonicity of the Weddell Gyre is indeed sensitive to changes in wind stress curl[28]. The role of barotropic dynamics and bottom Ekman layers has also been investigated[23]. Here we suggest, however, that the volume of underlying, denser, water masses has varied considerably, shifting the whole overlying water mass structure vertically, thus raising the level of the upper boundary of LWSDW and allowing more LWSDW to be exported north across the SSR. Several processes may be occurring concurrently but it appears that changes in WSBW volume presently dominate the water mass structure and LWSDW export, at least on multi-annual time scales.

Our data suggest that perturbations to the production of WSBW at the periphery of the Weddell Sea could be primarily responsible for large-scale variations in deep-water volume that are documented downstream in the Scotia Sea and beyond in the Atlantic Ocean. The time series necessary to fully diagnose such changes in WSBW production do not exist but observed climatic shifts in sea ice

concentration and ocean salinity near formation regions suggest this type of perturbation to be eminently plausible[29–32]. Changes in the properties of water masses advected into the Weddell Sea from the east could also contribute to some of these changes[33]. Enhanced monitoring of the formation regions of WSBW in the southern and western Weddell Sea could help constrain the processes responsible, if combined with concurrent monitoring of LWSDW exports as shown in this manuscript.

There are many important consequences to our observation of a stabilized and potentially rejuvenated export of dense waters from the Weddell Sea toward the Atlantic Ocean. The previously observed warming of AABW along much of the length of the Atlantic has been shown to have important implications for the planetary-scale heat budget and the thermal expansion component of sea level rise[3], as well as for cold-adapted benthic fauna vulnerable to even small temperature changes[34]. If, as was hypothesized, this warming was caused by a dwindling export of dense waters from high southern latitudes, our observation here of a reinvigoration of this export probably portends a cooling of the Atlantic abyssal waters in coming years. It should also be recalled that AABW circulates in the Atlantic as the lowest component of the Atlantic Meridional Overturning Circulation (AMOC); modelling studies have illustrated how changes in AABW export can influence not just the lower limb but the overall AMOC magnitude[8]. Consequently, the reinvigoration demonstrated here may have implications for the strength of the overturning circulation and thus for ocean heat and carbon sequestration. Finally, this observational study demonstrates a clear multi-annual reversal in AABW trends. Other studies of AABW around Antarctica[2,3,5,6] have been limited by data availability to seeking mainly monotonic changes in volume or properties on multi-annual time scales. The clearly resolved decline and recovery in LWSDW properties at the Scotia Sea section of A23 demonstrates both the value of frequent occupations of key hydrographic sections, and the need for sustained observations of bottom water source regions to understand the drivers of such large-scale changes and their global implications.

Online content

Any methods, additional references, Nature Research reporting summaries, source data, statements of code and data availability and associated accession codes are available at https://doi.org/10.1038/s41558-019-0561-2.

Received: 19 September 2018; Accepted: 25 July 2019;
Published online: 2 September 2019

References

1. Orsi, A. H., Johnson, G. C. & Bullister, J. L. Circulation, mixing, and production of Antarctic Bottom Water. *Prog. Oceanogr.* **43**, 55–109 (1999).
2. Johnson, G. C., McTaggart, K. E. & Wanninkhof, R. Antarctic Bottom Water temperature changes in the western south Atlantic from 1989 to 2014. *J. Geophys. Res. Oceans* **119**, 8567–8577 (2014).
3. Purkey, S. G. & Johnson, G. C. Antarctic Bottom Water warming and freshening: contributions to sea level rise, ocean freshwater budgets, and global heat gain. *J. Clim.* **26**, 6105–6122 (2013).
4. Purkey, S. G. & Johnson, G. C. Global contraction of Antarctic Bottom Water between the 1980s and 2000s. *J. Clim.* **25**, 5830–5844 (2012).
5. Menezes, V. V., Macdonald, A. M. & Schatzman, C. Accelerated freshening of Antarctic Bottom Water over the last decade in the Southern Indian Ocean. *Sci. Adv.* **3**, e1601426 (2017).
6. Rintoul, S. R. Rapid freshening of Antarctic Bottom Water formed in the Indian and Pacific oceans. *Geophys. Res. Lett.* **34**, L06606 (2007).
7. Bindoff, N. L. & Hobbs, W. R. Oceanography: deep ocean freshening. *Nat. Clim. Change* **3**, 864–865 (2013).
8. Patara, L. & Böning, C. W. Abyssal ocean warming around Antarctica strengthens the Atlantic overturning circulation. *Geophys. Res. Lett.* **41**, 3972–3978 (2014).
9. Johnson, G. C., Purkey, S. G. & Toole, J. M. Reduced Antarctic meridional overturning circulation reaches the North Atlantic ocean. *Geophys. Res. Lett.* **35**, L22601 (2008).
10. Johnson, G. C. Quantifying Antarctic Bottom Water and North Atlantic deep water volumes. *J. Geophys. Res. Oceans* **113**, C05027 (2008).
11. Sloyan, B. M. & Rintoul, S. R. The Southern Ocean limb of the global deep overturning circulation. *J. Phys. Oceanogr.* **31**, 143–173 (2001).
12. Jullion, L. et al. Decadal freshening of the Antarctic Bottom Water exported from the Weddell Sea. *J. Clim.* **26**, 8111–8125 (2013).
13. Meredith, M. P., Garabato, A. C. N., Gordon, A. L. & Johnson, G. C. Evolution of the deep and bottom waters of the Scotia Sea, Southern Ocean, during 1995–2005. *J. Clim.* **21**, 3327–3343 (2008).
14. Heywood, K. J., Naveira Garabato, A. C. & Stevens, D. P. High mixing rates in the abyssal Southern Ocean. *Nature* **415**, 1011–1014 (2002).
15. Jackett, D. R. & McDougall, T. J. A neutral density variable for the world's oceans. *J. Phys. Oceanogr.* **27**, 237–263 (1997).
16. Naveira Garabato, A. C., McDonagh, E. L., Stevens, D. P., Heywood, K. J. & Sanders, R. J. On the export of Antarctic Bottom Water from the Weddell Sea. *Deep Sea Res. Pt II* **49**, 4715–4742 (2002).
17. Naveira Garabato, A. C., Williams, A. P. & Bacon, S. The three-dimensional overturning circulation of the Southern Ocean during the WOCE era. *Prog. Oceanogr.* **120**, 41–78 (2014).
18. Firing, Y. L., McDonagh, E. L., King, B. A. & Desbruyères, D. G. Deep temperature variability in Drake Passage. *J. Geophys. Res. Oceans* **122**, 713–725 (2017).
19. Meijers, A. J. S. et al. Wind-driven export of Weddell Sea slope water. *J. Geophys. Res. Oceans* **121**, 7530–7546 (2016).
20. Fahrbach, E., Hoppema, M., Rohardt, G., Schröder, M. & Wisotzki, A. Decadal-scale variations of water mass properties in the deep Weddell Sea. *Ocean Dynam.* **54**, 77–91 (2004).
21. Sheen, K. L. et al. Rates and mechanisms of turbulent dissipation and mixing in the Southern Ocean: results from the diapycnal and isopycnal mixing experiment in the Southern Ocean (DIMES). *J. Geophys. Res. Oceans* **118**, 2774–2792 (2013).
22. Sheen, K. L. et al. Eddy-induced variability in Southern Ocean abyssal mixing on climatic timescales. *Nat. Geosci.* **7**, 577–582 (2014).
23. Meredith, M. P. et al. Synchronous intensification and warming of Antarctic Bottom Water outflow from the Weddell Gyre. *Geophys. Res. Lett.* **38**, L03603 (2011).
24. Su, Z., Stewart, A. L. & Thompson, A. F. An idealized model of Weddell Gyre export variability. *J. Phys. Oceanogr.* **44**, 1671–1688 (2014).
25. Polzin, K. L., Naveira Garabato, A. C., Abrahamsen, E. P., Jullion, L. & Meredith, M. P. Boundary mixing in Orkney Passage outflow. *J. Geophys. Res. Oceans* **119**, 8627–8645 (2014).
26. Thompson, A. F., Heywood, K. J., Schmidtko, S. & Stewart, A. L. Eddy transport as a key component of the Antarctic overturning circulation. *Nat. Geosci.* **7**, 879–884 (2014).
27. Coles, V. J., McCarney, M. S., Olson, D. B. & Smethie, W. M. Jr. Changes in Antarctic Bottom Water properties in the western South Atlantic in the late 1980s. *J. Geophys. Res. Oceans* **101**, 8957–8970 (1996).
28. Armitage, T. W. K., Kwok, R., Thompson, A. F. & Cunningham, G. Dynamic topography and sea level anomalies of the Southern Ocean: variability and teleconnections. *J. Geophys. Res. Oceans* **123**, 613–630 (2018).
29. Hellmer, H. H., Huhn, O., Gomis, D. & Timmermann, R. On the freshening of the northwestern Weddell Sea continental shelf. *Ocean Sci.* **7**, 305–316 (2011).
30. Haumann, F. A., Gruber, N., Münnich, M., Frenger, I. & Kern, S. Sea-ice transport driving Southern Ocean salinity and its recent trends. *Nature* **537**, 89–92 (2016).
31. Rye, C. D. et al. Rapid sea-level rise along the Antarctic margins in response to increased glacial discharge. *Nat. Geosci.* **7**, 732–735 (2014).
32. Daae, K., Darelius, E., Fer, I., Østerhus, S. & Ryan, S. Wind stress mediated variability of the Filchner Trough overflow, Weddell Sea. *J. Geophys. Res. Oceans* **123**, 3186–3203 (2018).
33. Kerr, R., Dotto, T. S., Mata, M. M. & Hellmer, H. H. Three decades of deep water mass investigation in the Weddell Sea (1984-2014): temporal variability and changes. *Deep Sea Res. Pt II* **149**, 70–83 (2018).
34. Sutherland, W. J. et al. A horizon scan of global conservation issues for 2012. *Trends Ecol. Evol.* **27**, 12–18 (2012).
35. Arhan, M., Heywood, K. J. & King, B. A. The deep waters from the Southern Ocean at the entry to the Argentine basin. *Deep Sea Res. Pt II* **46**, 475–499 (1999).
36. Stramma, L. & England, M. On the water masses and mean circulation of the south Atlantic ocean. *J. Geophys. Res. Oceans* **104**, 20863–20883 (1999).
37. Locarnini, R. A. et al. *World Ocean Atlas 2013* Vol. 1 (eds Levitus, S. & Mishonov, A.) (NOAA Atlas NESDIS Vol. 73, NOAA, 2013).
38. Zweng, M. M. et al. *World Ocean Atlas 2013* Vol. 2 (eds Levitus, S. & Mishonov, A.) (NOAA Atlas NESDIS Vol. 74, NOAA, 2013).
39. Garcia, H. E. et al. *World Ocean Atlas 2013* Vol. 3 (eds Levitus, S. & Mishonov, A.) (NOAA Atlas NESDIS Vol. 75, NOAA, 2014).
40. Garcia, H. E. et al. *World Ocean Atlas 2013* Vol. 4 (eds Levitus, S. & Mishonov, A.) (NOAA Atlas NESDIS Vol. 76, NOAA, 2014).

Acknowledgements

E.P.A., A.C.N.G. and M.P.M. were supported by Natural Environment Research Council (NERC) grant nos. NE/K012843/1 and NE/K013181/1 (Dynamics of the Orkney Passage Outflow). E.P.A., A.S.M., B.A.K., Y.L.F. and M.P.M. were supported by NERC grant no. NE/N018095/1 (Ocean Regulation of Climate by Heat and Carbon Sequestration and Transports, ORCHESTRA). K.P. was supported by NSF grant no. OCE-1536779. A.C.N.G. was supported by the Royal Society and the Wolfson Foundation. Collection of data on A23 and SR1b was supported by NERC National Capability funding including ORCHESTRA. Collection of data in Orkney Passage was supported by NERC National Capability funding including ORCHESTRA and was funded in part by the Climate Observation Division, Climate Program Office (FundRef no. 100007298), National Oceanic and Atmospheric Administration, US Department of Commerce. Computational resources for SOSE were provided by NSF XSEDE resource grant no. OCE130007.

Author contributions

E.P.A., A.S.M., M.P.M., B.A.K., Y.L.F., J.B.S. and B.A.H. contributed to data collection and interpretation. K.P. instigated this study with questions concerning the interpretation of the diminishing area of LWSDW along SR1b and A23. K.L.S. performed the kinetic energy anomaly analysis and generated Supplementary Fig. 3. E.P.A., A.S.M. and M.P.M. made the remaining figures and wrote the manuscript with contributions from all the remaining authors.

Competing interests

The authors declare no competing interests.

Additional information

Supplementary information is available for this paper at https://doi.org/10.1038/s41558-019-0561-2.

Reprints and permissions information is available at www.nature.com/reprints.

Correspondence and requests for materials should be addressed to E.P.A.

Peer review information: *Nature Climate Change* thanks Viviane Menezes and the other, anonymous, reviewer(s) for their contribution to the peer review of this work.

Publisher's note: Springer Nature remains neutral with regard to jurisdictional claims in published maps and institutional affiliations.

Methods

CTD data processing. For a detailed analysis of the CTD data errors on SR1b, see Jullion et al.[12]. The salinity errors on A23 are of comparable magnitude and those at SR4 have been estimated to be lower[20] but errors were computed here using the more conservative SR1b and A23 values. Salinities on all three sections have been corrected for standard seawater batch-to-batch offsets (Kawano et al.[41], with recent additions from H. Uchida, personal communications, 2015 and 2018), as per Firing et al.[18].

To calculate the water mass areas, station positions are projected onto a piecewise linear section in Mercator projection; the location of each section was chosen based on the initial occupation of each section; most of the coordinates initially were chosen on rhumb lines. The horizontal (distance) coordinate is calculated by finding the position along this line that minimizes the distance normal to the line. Neutral densities (calculated using the gamma_n Fortran routines of Jackett and McDougall[15], interfaced with Matlab) are linearly interpolated (horizontally and vertically) onto a grid with a horizontal resolution of 1 km and a vertical resolution of 2 m, with profile data extrapolated in the vertical (using the first/last measured value) to the surface or bottom if necessary. A depth mask is then applied, based on Smith and Sandwell[42] (v. 16.1, December 2013). The number of grid cells that fall in each density range (and latitude/longitude range, for A23 and SR4, respectively) is then summed and multiplied by the grid cell area to obtain the water mass area.

The error bars in Fig. 2 are calculated to take into account both the accuracy of the neutral density calculation itself (as described in appendix B of Jackett and McDougall[15]), the underlying accuracy of the temperature and salinity measurements, and the errors arising from the variable station spacing. LWSDW area perturbations are calculated corresponding to salinity offsets of ±0.002 and temperature offsets of ±0.001 °C, along with the lower and upper error ranges of neutral density calculated by the gamma_n software from each section. The resulting ranges in LWSDW areas from salinity and neutral density are of the same magnitude; however, in the LWSDW layer, the neutral density error range is skewed toward lower values, while the salinity and temperature are approximately symmetric around zero. This results in a bias toward lower LWSDW area estimates. The errors resulting from varying station spacing were estimated by subsampling the 1/6° Southern Ocean State Estimate[43] (SOSE) to match the station locations from each occupation of a section. The difference between the LWSDW area based on this subset and the area computed using the full model grid is calculated for each 5-day average from the 6-yr SOSE run (2005–2010; iteration 100); the 5th and 95th percentiles of these differences are added to the errors from neutral density, salinity and temperature described above. The largest errors from station spacing correspond to the occupations of the sections with the lowest spatial resolution (for example the 2005 and the first 2014 occupation of A23) and cause a bias toward higher values, as the set of stations on those sections tend to under-sample the denser water masses. The effect of salinity and neutral density errors is largest on the sections with the highest LWSDW areas; these are generally the dominant sources of error (by a factor of 5), except for the two coarser sections, where the resolution error is slightly larger. Errors resulting from temperature variations are an order of magnitude smaller, owing largely to the reduced sensitivity of density to temperature at high latitudes (in cold temperatures). SOSE has no LWSDW on SR1b; instead the area of Upper WSDW (UWSDW), scaled by the average observed ratio of LWSDW to UWSDW areas on the section, was used.

Moored current meter transports. Transports of LWSDW through Orkney Passage were calculated by linearly interpolating the mooring temperatures, salinities and currents perpendicular to the direction of the mooring array onto a grid with a horizontal resolution of about 350 m and a vertical resolution of 8 m. For instruments measuring only temperature, salinities were estimated using a linear temperature–salinity relationship obtained from the remaining instruments on that particular mooring. Neutral density was calculated from the gridded data and velocities were integrated over the area with neutral densities matching the criteria for LWSDW.

To estimate the effect of an increase in Orkney Passage transport on the A23 LWSDW area, the 2013–2015 transport anomaly of 0.3 Sv was assumed to uniformly raise the $\gamma^n = 28.31\,\mathrm{kg\,m^{-3}}$ surface across the Scotia Sea. The areal extent of this water mass has been estimated to be $5.85\times10^{11}\,\mathrm{m^2}$ (World Ocean Atlas 2013[37,38] average between 1955 and 2012) or $7\times10^{11}\,\mathrm{m^2}$ (1990s[14]), with a tendency towards lower extent in later years. The observed increase of 0.3 Sv inflow to the Scotia Sea would result in a 27–76 m rise in the height of the bounding isopycnal over 2 yr. Assuming that LWSDW covers a meridional extent of 300 ± 64 km on the Scotia Sea part of the A23 section, this translates into an increase in the LWSDW area of $8.1\pm1.7\times10^6\,\mathrm{m^2}$ to $2.3\pm0.5\times10^7\,\mathrm{m^2}$.

Surface eddy kinetic energy. Following Sheen et al.[22], we calculate the surface kinetic energy anomaly, $\mathrm{KE_{anom}}$, as a proxy for surface eddy kinetic energy. $\mathrm{KE_{anom}}$ was calculated from daily Ssalto/Duacs altimetry mapped surface geostrophic velocity as $\mathrm{KE_{anom}} = \left[(u-\bar{u})^2+(v-\bar{v})^2\right]/2$, where u and v are the zonal and meridional components of the surface geostrophic velocity anomaly, respectively, and the overbar represents the temporal mean since the start of December 1993 (~23-yr altimetric time series). The time series of average $\mathrm{KE_{anom}}$ between 54–62° S and 30–50° W (Supplementary Fig. 3), were low-pass filtered using a sixth-order Butterworth filter with a cut-off frequency of 45 d. This 45-d time scale was chosen because Sheen et al.[22] find surface $\mathrm{KE_{anom}}$ is related to abyssal turbulence on time periods of 1–3 months, typical of the eddy field.

The two-satellite merged product is based on only two missions at any given time: Jason-2/AltiKa or Jason-2/Cryosat-2 or Jason-2/Envisat or Jason-1/Envisat or Topex/Poseidon/ERS, with the same groundtrack, and provides a stable sampling pattern. Because the all-satellite merged product uses all missions available at a given time, the time series produced is not homogeneous and hence is inappropriate for determining long-term changes; consequently, we use the homogeneous two-satellite product here.

Wind stress and wind stress curl. The wind stress and wind stress curl over the Weddell Gyre and SSR plotted in Supplementary Fig. 4 were calculated using the ERA-Interim reanalysis product[44] monthly-mean wind stress between 1979 and 2017 and were averaged over the areas between 60–0° W, 62–70° S and 60-20° W, 60–65° S for the Weddell Gyre and SSR, respectively.

Further discussion. Here, we discuss in more detail the other candidate mechanisms considered as potential contributors to the LWSDW changes seen on the A23 section.

The relatively infrequent sampling on A23 before 2010, combined with the relatively short residence time of LWSDW in the Scotia Sea, means that the possibility of aliasing the interannual variability during this period of decline cannot be excluded completely. However, the intervals between section occupations since 2010 are shorter than the residence time scale for this water mass, on the order of 2.5 yr[14], and thus we can be confident that the recovery in LWSDW observed since 2014 is real and not an artefact of aliasing.

Concerning possibility 2 above, that they are caused by changes in water mass properties and hence density, Jullion et al.[12] observed a decrease in the salinity of UWSDW (defined by $28.26<\gamma^n<28.31\,\mathrm{kg\,m^{-3}}$) on SR1b equivalent to −0.007 from 1993 to 2011. SR1b LWSDW also displays a salinity trend of −0.0025 per decade (see Supplementary Fig. 2). On the A23 section in the Scotia Sea, LWSDW freshening is smaller in amplitude (0.0016 per decade), the trend is not significant for the period of the decline and the salinities appear to have continued decreasing toward the present (two of the three lowest LWSDW salinity anomalies observed on the section were in the last two occupations of the section); thus, we do not believe that salinity changes can be responsible for the variability observed. The decrease in LWSDW potential temperature on A23 is equivalent to −0.008 °C per decade, also smaller than the equivalent trend on SR1b of −0.0116 °C per decade.

In Fig. 2, the temperature and salinity anomalies for each occupation of the sections (as shown in Supplementary Fig. 2) have been subtracted from the data, individually and together, and the LWSDW areas recomputed, resulting in the red (temperature only), green (salinity only) and black (both) bars. The density effects of freshening and cooling on the A23 section are not large enough in magnitude to account for the significant downward trend in the area of LWSDW on A23 observed up to 2014, nor for its subsequent strong recovery. Consequently, possibility 2 is unlikely to be a major causal factor in the LWSDW changes observed in the Scotia Sea.

Concerning possibility 3, that the LWSDW changes in the Scotia Sea might be caused by changes in its rate of removal, it should be noted that the direct export of this water mass from the Scotia Sea is facilitated by diapycnal mixing, since the depths at which the water resides are blocked by topography around the northern and eastern flanks of the basin[45]. Consequently, for the observed trend in LWSDW area to be influenced by changing outflow from the Scotia Sea, changes in the rates of deep diapycnal mixing therein would be required. Unfortunately, direct observations of deep-ocean mixing over time are lacking, making it difficult to make definitive statements concerning trends. A time series of deep-ocean turbulent dissipation using velocity and hydrographic measurements from the SR1b section[22], however, showed that strong, deep diapycnal mixing was predominantly collocated with the fronts of the Antarctic circumpolar current, and that changes in mixing were forced by changes in the mesoscale eddy field. Such enhanced deep mixing is unlikely to explain the changes at A23, as the highest levels of eddy variability associated with the polar and sub-Antarctic fronts are located north of the LWSDW extent in the Scotia Sea. Despite this, following Sheen et al.[22], who showed that surface kinetic energy anomaly ($\mathrm{KE_{anom}}$) is related to abyssal turbulent mixing, we examined the $\mathrm{KE_{anom}}$ over the Scotia Sea (Supplementary Fig. 3) and found that, in addition to substantial interannual variability, there has been an increase in $\mathrm{KE_{anom}}$ since 1993 and particularly since 2006. However, there is no significant decrease in $\mathrm{KE_{anom}}$ post-2013 and in fact it is higher then than over most of the rest of the record. This suggests that a decrease in mixing cannot be a major cause of the strong recovery in LWSDW after this period.

Accordingly, the balance of evidence strongly suggests that the change in volume of LWSDW in the Scotia Sea is predominantly driven by changes in the supply of this water mass from the Weddell Sea via Orkney Passage, with changes in its hydrographic properties and its diapycnal mixing playing secondary or negligible roles.

Data availability

CTD data were collected on UK, US and German research cruises; these data are available at CCHDO (http://cchdo.ucsd.edu) for US and some UK cruises, BODC (http://www.bodc.ac.uk) for UK cruises and PANGAEA (http://www.pangaea.de) for German cruises[46–54]; links to the data are given in Supplementary Table 1. Mooring data from Orkney Passage are available from BODC at https://www.bodc.ac.uk/data/bodc_database/nodb/data_collection/6565/.
The altimeter products were produced by Ssalto/Duacs and distributed by Aviso, with support from CNES (https://www.aviso.altimetry.fr). ERA-interim reanalysis data are available from the ECMWF (https://www.ecmwf.int/en/research/climate-reanalysis/era-interim). SOSE data are available from http://sose.ucsd.edu/. GEBCO_2014 bathymetry data are available from https://www.gebco.net/.

References

41. Kawano, T. et al. The latest batch-to-batch difference table of standard seawater and its application to the WOCE onetime sections. *J. Oceanogr.* **62**, 777–792 (2006).
42. Smith, W. H. F. & Sandwell, D. T. Global sea floor topography from satellite altimetry and ship depth soundings. *Science* **277**, 1956–1962 (1997).
43. Mazloff, M. R., Heimbach, P. & Wunsch, C. An eddy-permitting Southern Ocean state estimate. *J. Phys. Oceanogr.* **40**, 880–899 (2010).
44. Dee, D. P. et al. The ERA-Interim reanalysis: configuration and performance of the data assimilation system. *Q. J. R. Meteorol. Soc.* **137**, 553–597 (2011).
45. Naveira Garabato, A. C., Heywood, K. J. & Stevens, D. P. Modification and pathways of Southern Ocean deep waters in the Scotia Sea. *Deep Sea Res. Pt II* **49**, 681–705 (2002).
46. Fahrbach, E. & Rohardt, G. Physical Oceanography during POLARSTERN Cruise ANT-VIII/2 (WWGS) on Section SR02 and SR04. *PANGAEA* https://doi.org/10.1594/PANGAEA.742580 (1990).
47. Fahrbach, E. & Rohardt, G. Physical Oceanography during POLARSTERN Cruise ANT-IX/2 on Section SR04. *PANGAEA* https://doi.org/10.1594/PANGAEA.735277 (1991).
48. Fahrbach, E. & Rohardt, G. Physical Oeanography during POLARSTERN Cruise ANT-X/7 on Section SR04. *PANGAEA* https://doi.org/10.1594/PANGAEA.742651 (1993).
49. Fahrbach, E. & Rohardt, G. Physical Oceanography during POLARSTERN Cruise ANT-XIII/4 on Section S04A. *PANGAEA* https://doi.org/10.1594/PANGAEA.738489 (1996).
50. Fahrbach, E. & Rohardt, G. Physical Oceanography during POLARSTERN Cruise ANT-XV/4 (DOVETAIL) on Section SR04. *PANGAEA* https://doi.org/10.1594/PANGAEA.742626 (1998).
51. Rohardt, G. Physical Oceanography during POLARSTERN Cruise ANT-XXII/3. *PANGAEA* https://doi.org/10.1594/PANGAEA.733664 (2010).
52. Fahrbach, E. & Rohardt, G. Physical Oceanography during POLARSTERN Cruise ANT-XXIV/3. *PANGAEA* https://doi.org/10.1594/PANGAEA.733414 (2008).
53. Rohardt, G., Fahrbach, E. & Wisotzki, A. Physical Oceanography during POLARSTERN Cruise ANT-XXVII/2. *PANGAEA* https://doi.org/10.1594/PANGAEA.772244 (2011).
54. Rohardt, G. Physical Oceanography during POLARSTERN Cruise ANT-XXIX/2. *PANGAEA* https://doi.org/10.1594/PANGAEA.817255 (2013).